AJNR

4D DSA for Dynamic Visualization of Cerebral Vasculature: A Single-Center Experience in 26 Cases

S. Lang, P. Gölitz, T. Struffert, J. Rösch, K. Rössler, M. Kowarschik, C. Strother and A. Doerfler

AJNR Am J Neuroradiol 2017, 38 (6) 1169-1176
doi: https://doi.org/10.3174/ajnr.A5161
http://www.ajnr.org/content/38/6/1169

4D DSA for Dynamic Visualization of Cerebral Vasculature: A Single-Center Experience in 26 Cases

S. Lang, P. Gölitz, T. Struffert, J. Rösch, K. Rössler, M. Kowarschik, C. Strother, and A. Doerfler

ABSTRACT

BACKGROUND AND PURPOSE: 4D DSA allows acquisition of time-resolved 3D reconstructions of cerebral vessels by using C-arm conebeam CT systems. The aim of our study was to evaluate this new method by qualitative and quantitative means.

MATERIALS AND METHODS: 2D and 4D DSA datasets were acquired in patients presenting with AVMs, dural arteriovenous fistulas, and cerebral aneurysms. 4D DSA was compared with 2D DSA in a consensus reading of qualitative and quantitative parameters of AVMs (eg, location, feeder, associated aneurysms, nidus size, drainage, Martin-Spetzler Score), dural arteriovenous fistulas (eg, fistulous point, main feeder, diameter of the main feeder, drainage), and cerebral aneurysms (location, neck configuration, aneurysmal size). Identifiability of perforators and diameters of the injection vessel (ICA, vertebral artery) were analyzed in 2D and 4D DSA. Correlation coefficients and a paired *t* test were calculated for quantitative parameters. The effective patient dose of the 4D DSA protocol was evaluated with an anthropomorphic phantom.

RESULTS: In 26 patients, datasets were acquired successfully (AVM = 10, cerebral aneurysm = 10, dural arteriovenous fistula = 6). Qualitative and quantitative evaluations of 4D DSA in AVMs (nidus size: $r = 0.99$, $P = .001$), dural arteriovenous fistulas (diameter of the main feeder: $r = 0.954$, $P = .03$), and cerebral aneurysms (aneurysmal size: $r = 1$, $P = .001$) revealed nearly complete accordance with 2D DSA. Perforators were comparably visualized with 4D DSA. Measurement of the diameter of the injection vessel in 4D DSA was equivalent to that in 2D DSA ($P = .039$). The effective patient dose of 4D DSA was 1.2 mSv.

CONCLUSIONS: 4D DSA is feasible for imaging of AVMs, dural arteriovenous fistulas, and cerebral aneurysms. 4D DSA offers reliable visualization of the cerebral vasculature and may improve the understanding and treatment of AVMs and dural arteriovenous fistulas. The number of 2D DSA acquisitions required for an examination may be reduced through 4D DSA.

ABBREVIATIONS: dAVF = dural arteriovenous fistula; IQ = image quality; MS-S = Martin-Spetzler Score; VA = vertebral artery

The current criterion standard for visualization of the cerebral vasculature is DSA by acquisition of dynamic 2D series (2D DSA). Additional 3D rotational angiography is used for the diagnostic work-up of arteriovenous malformations, dural arteriovenous fistulas (dAVFs), and cerebral aneurysms.[1-3] Despite the high image quality of 2D DSA and the opportunity to visualize vessels at any angle by 3D DSA, this method is limited due to overlap of arterial and venous structures.[4,5] This may impair recognition of anatomic details, especially in complex pathologies. Despite the use of 3D DSA images for improved spatial understanding, 2D DSA series are still necessary to better understand the dynamics of blood flow. The more complex the pathology, the more 2D projections might be necessary. It would be obligatory to limit the number of 2D series to reduce the effective patient dose and contrast volumes. Therefore, a technique that combines flow information with 3D imaging would be desirable in the visualization of the cerebral vasculature.

A novel method has been described recently, which is based on the rotational acquisitions of mask and fill projection images and generates a static 3D DSA dataset and a series of time-resolved 3D vascular volumes (4D DSA), that illustrates the contrast in- and outflow with time. In 2013, Davis et al[6] demonstrated the technical feasibility of this new technique. Meanwhile, Sandoval-Garcia et al[7,8]

Received September 2, 2016; accepted after revision January 23, 2017.

From the Departments of Neuroradiology (S.L., P.G., T.S., J.R., A.D.) and Neurosurgery (K.R.), University of Erlangen-Nuremberg, Erlangen, Germany; Angiography & Interventional X-Ray Systems (M.K.), Siemens Healthcare GmbH, Forchheim, Germany; and Department of Radiology (C.S.), University of Wisconsin School of Medicine and Public Health, Madison, Wisconsin.

The Department of Neuroradiology, University of Erlangen-Nuremberg has a research agreement with Siemens Healthcare GmbH, Forchheim, Germany.

Please address correspondence to Stefan Lang, MD, Department of Neuroradiology, University of Erlangen-Nuremberg, Schwabachanlage 6, 91054 Erlangen, Germany; e-mail: Stefan.Lang3@uk-erlangen.de

http://dx.doi.org/10.3174/ajnr.A5161

have shown the clinical feasibility of 4D DSA both in a canine model and in patients, with promising results. Recently, the detailed analysis of dAVFs and AVMs with 4D DSA of Lescher et al[9] demonstrated a significantly improved visualization of a fistulous point of the dAVF or a nidus of the AVM by using 4D DSA; in many cases, 4D DSA even came close to superselective angiography.

In this article, we present our initial clinical experience with 4D DSA in the diagnostic work-up of vascular malformations by comparing 4D with 2D DSA. Furthermore, we provide information about the effective radiation dose for this new technique.

MATERIALS AND METHODS

Patients

Patients presenting with AVMs, dural fistulas, or cerebral aneurysms were included in this study. Ethics committee approval was obtained before this study, and informed consent was obtained from all patients enrolled.

4D DSA

4D DSA refers to a novel acquisition method to create time-resolved datasets of vascular volumes by using C-arm conebeam CT systems.[6,10] This is accomplished with a 3D DSA acquisition protocol that comprises 2 rotational runs: mask and fill. Proper timing of the contrast injection allows visualization of the inflow of contrast in any projection. The enlarged rotational angle in comparison with established 3D DSA programs (5s DSA program; Siemens, Erlangen, Germany) generates a sufficiently large number of projections for an adequate time duration that is sufficient to follow the contrast bolus throughout the vasculature.

We used an acquisition protocol (12s 4D DSA program, Siemens) that applies 2 runs (native and fill run) of 12 seconds each. Each run yields a total of 304 projection images over a rotational angle of 260°. The detector dose per projection image is selected as 0.36 μGy (70 kV, 1240 × 960 detector elements with 2-by-2 binning of pixels, projection on a 30 × 40 cm flat panel size, increment of 0.85°/frame, frame rate of 30 frames/s).

Postprocessing generates a conventional 3D DSA reconstruction before the reconstruction of the time-resolved series of volumes (4D DSA). The subsequent reconstruction of 4D DSA volumes is based on embedding the temporal flow information extracted from the rotational projections of the fill run to the preliminary reconstructed conventional 3D DSA dataset. Technically, this computational step is referred to a "constrained reconstruction."[10] With the 4D DSA prototype software, each projection of the rotational fill run leads to a temporal volume of the 4D DSA image series. Hence, the time-resolved series of vascular volumes covers 304 time-steps, providing a temporal solution of 12 seconds in total. On the basis of the combination of a conventional 3D DSA dataset with flow information from these 304 projection images, 4D DSA can provide "any view at any time."[6]

Data Acquisition and Postprocessing

Cerebral angiography (including 2D DSA and 4D DSA) was performed by using a biplane flat panel detector angiographic system (Artis zee biplane; Siemens). By standard angiographic methods (via the transfemoral route), a diagnostic catheter (5F) was positioned in the proximal internal carotid artery or in the vertebral artery (VA) to obtain standard posteroanterior and lateral projections (2D DSA). After we adjusted the C-arm (as known from other flat-detector acquisition protocols), we obtained the rotational scan by using the identical 4D DSA acquisition protocol provided by the manufacturer in all patients. An initial rotational scan (native "mask run") is followed by a second rotational scan (contrast-enhanced "fill run"). According to our examination protocol, manual injection of the contrast medium was started after initiation of the fill run for illustration of the contrast material inflow into the cerebral vasculature. The injection was maintained for 8 seconds. Then, the injection was stopped to display venous outflow as well. The total contrast volume was 15 mL (iopamidol, Imeron 300; Bracco, Milan, Italy). The angiographic data were transferred to a dedicated workstation (syngo X Workplace; Siemens) running prototype software for postprocessing of 4D DSA images. According to standardization and previous experience, we used reconstruction parameters identical to those used in conventional 3D DSA (kernel type: "edge enhanced"; image characteristics: "smooth"; mode of reconstruction: "subtracted"; 512 × 512 image matrix). Before image interpretation, postprocessing of 4D DSA datasets requires, depending on selected voxel size, between 3 minutes 30 seconds for aneurysms and 6 minutes 45 seconds for AVMs or dAVFs. On the basis of static and time-resolved reconstructions of 4D DSA, we determined the best projections for subsequent enlarged oblique 2D series ("target projections").

Data Evaluation

Any 2D and 4D data were anonymized and stored in random order. 2D DSA series as the criterion standard were analyzed with regular viewing software. The range of 2D DSA series considered for evaluation was confined to the injection vessel of the corresponding 4D DSA. Image evaluation of 4D DSA was performed with volume-rendered, multiplanar, and MIP reconstructions by using the syngo InSpace plug-in of the prototype software (Siemens).

Analysis of 2D and 4D DSA datasets was performed by 2 experienced neuroradiologists in a consensus reading, blinded to clinical information.

Image Quality

All 2D and 4D DSA datasets were evaluated by the 2 neuroradiologists for parameters that compromise image and diagnostic quality (eg, movement). The quality of the acquired 2D and 4D DSA datasets was assessed in a consensus reading by using a 5-fold scaled grading system: 4 = excellent (high contrast, no artifacts); 3 = good (high contrast; minimal artifacts, eg, due to movement or metallic implants); 2 = compromised (eg, noticeable movement artifacts and/or reduced homogeneity of the vessel contrast); 1 = heavily compromised (low contrast and/or strong movement artifacts); 0 = not diagnostic (vasculature is not differentiable due to heavy artifacts and/or missing contrast).

Qualitative and Quantitative Evaluation of the 2D and 4D DSA Datasets

AVM. For qualitative assessment of AVM involvement of an eloquent brain area, origin of the main feeders, venous drainage

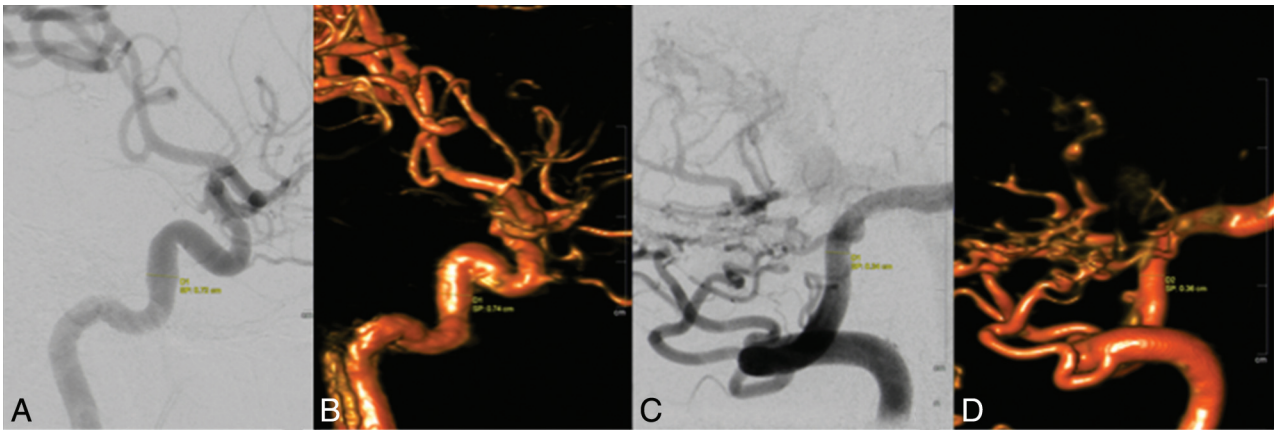

FIG 1. Images show measurements in 2D (*A* and *C*) and 4D DSA (*B* and *D*) of the vessel diameters of the ICA and VA in lateral projections of the anterior left-sided circulation and the posterior circulation, respectively. Comparable vessel diameters can be evaluated for the ICA (2D DSA = 0.72 cm, 4D DSA = 0.74 cm) and the VA (2D DSA = 0.34 cm, 4D DSA = 0.36 cm).

(superficial, deep), and pathologies of venous vessels (stenosis, pouch) were evaluated in both 2D and 4D DSA datasets with standard and working projections. As quantitative parameters, the number of feeders (with standard and working projections), the number of associated flow-related/intranidal aneurysms (with standard and working projections), and the maximum diameter of the nidus (with a strict lateral projection) were analyzed in both modalities. On the basis of the collected data, the Martin-Spetzler Scores (MS-S) for the 2D and 4D DSA datasets were calculated.

dAVF. For qualitative assessment of the origin of the main feeders of the dAVFs (eg, internal carotid artery, ophthalmic artery, posterior meningeal artery), the primary vessel of venous drainage (vein or sinus), the localization of the fistulous point (anterior/middle/posterior cranial fossa), and drainage of the fistula (transverse-sigmoid, petrous, superior sagittal, and straight sinuses) were evaluated in both 2D and 4D DSA datasets by using standard and working projections. As a quantitative parameter, the maximum diameter of the main feeder was measured in both modalities by using a strict lateral projection.

Cerebral Aneurysms. For qualitative assessment of cerebral aneurysms, location (parent vessel, eg, internal carotid artery, middle cerebral artery, basilar artery), neck configuration (small, <5 mm; medium, >5 mm/<10 mm; large, >10 mm; not definable), and aneurysmal configuration (sacciform, fusiform) were evaluated in both 2D and 4D DSA datasets by using standard and working projections. As a quantitative parameter, the maximal aneurysmal size was measured in both modalities by using a working projection.

Qualitative Evaluation of Perforators

4D DSA was compared with 2D DSA concerning visualization of the smallest vessels (perforators): exemplarily and due to standardization, the identifiability of lenticulostriate and thalamoperforating arteries (in datasets of the anterior and posterior circulation, respectively) was assessed by both readers with standard projections.

Quantitative Assessment of the Injection Vessel

To compare 4D DSA with 2D DSA in terms of accuracy, both readers measured the maximum-diameter vessel with standard tools of the prototype workstation in strict lateral projections. Measurement for datasets of the anterior circulation was performed via the ICA at the C4 segment according to the Bouthillier classification, as exemplarily demonstrated in Fig 1. Measurement for datasets of the posterior circulation was performed via the VA at the V4 segment.

Statistical Analysis

Qualitative parameters (eg, location of the pathology, origin of the main feeder, drainage, and so forth) were analyzed by using descriptive statistics only. Quantitative parameters (measurements of the nidus size, aneurysmal size, diameters of the main feeder of the dural fistula, and injection vessels) were tested for normal distribution by using the D'Agostino-Pearson test (if $P > .05$ normality was accepted). The Pearson correlation coefficient (r) was used to evaluate correlations for linear scaled variables (the number of AVM feeders, the number of intranidal aneurysms, nidus size, the main feeder of the fistula, aneurysm size); the Kendall $\tau\,\beta$ was used for ordinal scaled variables (image quality [IQ], number of flow-associated aneurysms). A paired t test was performed for statistical analysis of the diameter of the injection vessels.

Dose Measurement

We used an anthropomorphic phantom (Alderson RANDO; Radiology Support Devices, Long Beach, California), as previously described, and thermoluminescent dosimeters (Thermo Fisher Scientific, Waltham, Massachusetts) to measure the effective dose to the patient of the new 12s 4D DSA protocol.[11-13]

RESULTS

Patients

Twenty-six patients (mean age, 55.04 ± 15 years; 8 women and 18 men) with 10 AVMs, 10 cerebral aneurysms, and 6 dAVFs were enrolled in our study. Six patients (23%) had intracranial hemorrhage; 20 patients (77%) had an incidental finding. In all cases, a 4D DSA dataset was acquired in addition to conventional 2D DSA. Contrast medium was applied in 21 patients via the ICA (81%) and in 5 patients via the VA (19%).

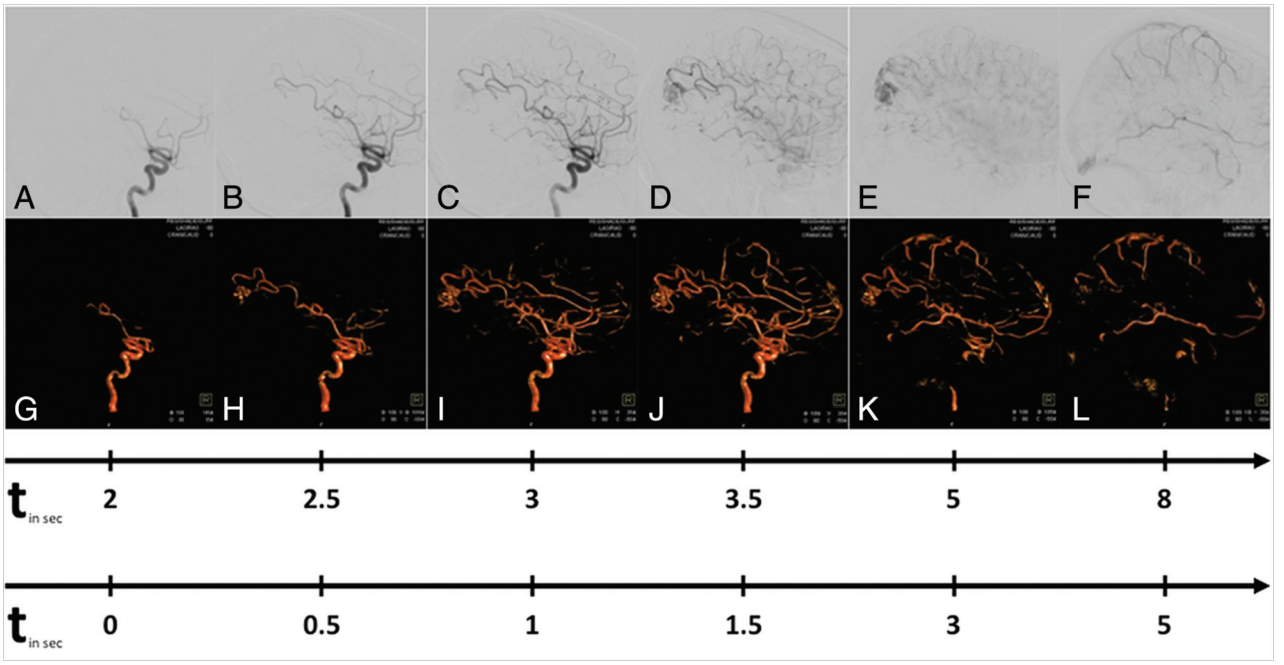

FIG 2. Illustrative case 1. MR imaging reveals an incidental AVM of the right occipital lobe in a 47-year-old man with persistent headache. This case demonstrates the potential of 4D DSA (*G–L*, *lower row*) to illustrate sequential filling of cerebral vessels concordant with 2D DSA (*A–F*, *upper row*). Early 4D volumes show both feeders originating from the posterior parietal artery and the initial enhancement of the nidus. Later volumes of 4D DSA display the compact nidus. Flow-associated/intranidal aneurysms and a direct AVF can be excluded. Late volumes illustrate exclusive venous outflow via superficial veins and the superior sagittal sinus (Martin-Spetzler Score 2). The upper timeline shows the real-time of the filling phases; the lower timeline shows the temporal differences between each image.

Image Quality

In all cases ($n = 26$), 4D DSA yielded diagnostic quality (average$_{2D} = 3.88 \pm 0.43$; average$_{4D} = 3.85 \pm 0.46$; $\tau_{IQ} = 0.78$, $P = .001$). The IQ of three 2D and three 4D datasets was limited because of motion artifacts.

Qualitative and Quantitative Evaluation of Vascular Pathologies

AVM. Ten 4D datasets were successfully acquired by injection via the ICA ($n_{left} = 8$, $n_{right} = 2$). Analysis of 4D datasets revealed identical results concerning qualitative parameters: effect on eloquent brain areas ($n_{2D} = 5$, $n_{4D} = 5$), main feeder of the AVM (MCA: $n_{2D} = 10$, $n_{4D} = 10$), venous drainage (superficial: $n_{2D} = 7$, $n_{4D} = 7$; deep: $n_{2D} = 3$, $n_{4D} = 3$), and pathologies of venous vessels (stenosis: $n_{2D} = 1$, $n_{4D} = 1$; pouch: $n_{2D} = 2$, $n_{4D} = 2$). The number of arterial feeders ($n_{2D} = 26$, $n_{4D} = 26$; $r = 1$, $P = .001$) was rated identically; the number of associated aneurysms (flow-related: $n_{2D} = 2$, $n_{4D} = 2$; $\tau = 1$, $P = .001$; intranidal: $n_{2D} = 7$, $n_{4D} = 8$; $r = 0.9$, $P = .001$) was rated nearly identically (compare with Fig 2). Measurement of the nidus size in the acquired 4D datasets (2.78 ± 1.4 cm) showed a strong correlation ($r = 0.99$, $P = .001$) to the 2D datasets (2.79 ± 1.4 cm). Martin-Spetzler Scores were identical for AVMs in 2D and 4D DSA ($n_{MS\text{-}S1} = 2$; $n_{MS\text{-}S2} = 4$; $n_{MS\text{-}S3} = 3$; $n_{MS\text{-}S4} = 1$).

dAVF. In total, six 4D datasets were successfully acquired by selective injection via the ICA ($n = 4$) and the VA ($n = 2$). Analysis of 4D datasets revealed identical results with regard to qualitative parameters (compare with Fig 3): the origin of the main feeders (ICA: $n_{2D} = 2$, $n_{4D} = 2$; ophthalmic artery: $n_{2D} = 2$, $n_{4D} = 2$; posterior meningeal artery: $n_{2D} = 2$, $n_{4D} = 2$), localization of the fistulous point (anterior cranial fossa: $n_{2D} = 2$, $n_{4D} = 2$; middle cranial fossa: $n_{2D} = 2$, $n_{4D} = 2$; posterior cranial fossa: $n_{2D} = 2$, $n_{4D} = 2$), primary vessel of venous drainage (vein: $n_{2D} = 5$, $n_{4D} = 5$; sinus: $n_{2D} = 1$, $n_{4D} = 1$), and drainage of the fistula (transverse sigmoid sinus: $n_{2D} = 2$, $n_{4D} = 2$; petrous sinus: $n_{2D} = 1$, $n_{4D} = 1$; straight sinus: $n_{2D} = 1$, $n_{4D} = 1$; superior sagittal sinus: $n_{2D} = 2$, $n_{4D} = 2$). Measurement of the main feeder of the fistula in the acquired 4D datasets (0.12 ± 0.04 cm) showed a strong correlation ($r = 0.954$, $P = .003$) to the 2D datasets (0.11 ± 0.03 cm).

Cerebral Aneurysms. In total, 10 4D datasets were successfully acquired by selective injection via the ICA ($n = 7$) and the VA ($n = 3$). Analysis of 4D datasets revealed identical results for qualitative parameters (compare with Fig 4): location (basilar artery: $n_{2D} = 3$, $n_{4D} = 3$; right ICA: $n_{2D} = 5$, $n_{4D} = 5$; left ICA: $n_{2D} = 2$, $n_{4D} = 2$), aneurysmal configuration (sacciform: $n_{2D} = 9$, $n_{4D} = 9$; fusiform: $n_{2D} = 1$, $n_{4D} = 1$), and aneurysmal neck (small: $n_{2D} = 4$, $n_{4D} = 4$; medium: $n_{2D} = 3$, $n_{4D} = 3$; large: $n_{2D} = 2$, $n_{4D} = 2$; not definable: $n_{2D} = 1$, $n_{4D} = 1$). Measurement of the aneurysm size in the acquired 4D datasets (1.33 ± 0.9 cm) showed a strong correlation ($r = 1$, $P = .001$) to the 2D datasets (1.34 ± 0.98 cm).

Qualitative Evaluation of Perforators

Analysis of 4D datasets revealed nearly identical results compared with 2D DSA with regard to visualization of perforators ($n_{\text{lenticulostriate arteries 2D}} = 19$, $n_{\text{lenticulostriate arteries 4D}} = 18$; $n_{\text{thalamoperforating arteries 2D}} = 5$, $n_{\text{thalamoperforating arteries 4D}} = 5$; examples are shown in Figs 5 and 6). In 2 cases, lenticulostriate

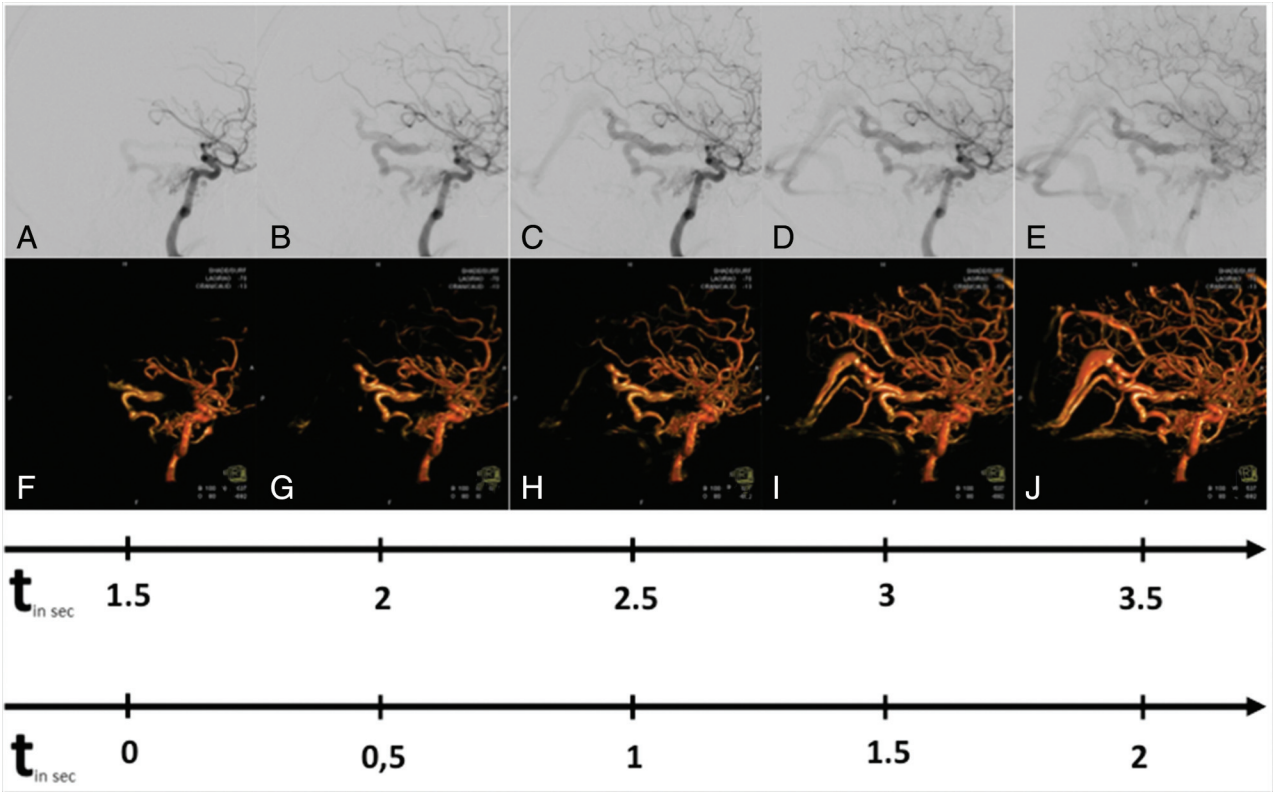

FIG 3. Illustrative case 2. This 39-year-old male patient has left-sided pulsatile tinnitus. Comparable with 2D DSA (*A–E*, *upper row*), 4D DSA (*F–J*) illustrates the early enhancement of a fistulous network on the left-sided skull base originating from the distal ICA. Later volumes show the early filling of the straight sinus via the ectatic basal vein. The upper timeline shows, in real-time, the filling phases; the lower timeline shows the temporal differences between each image.

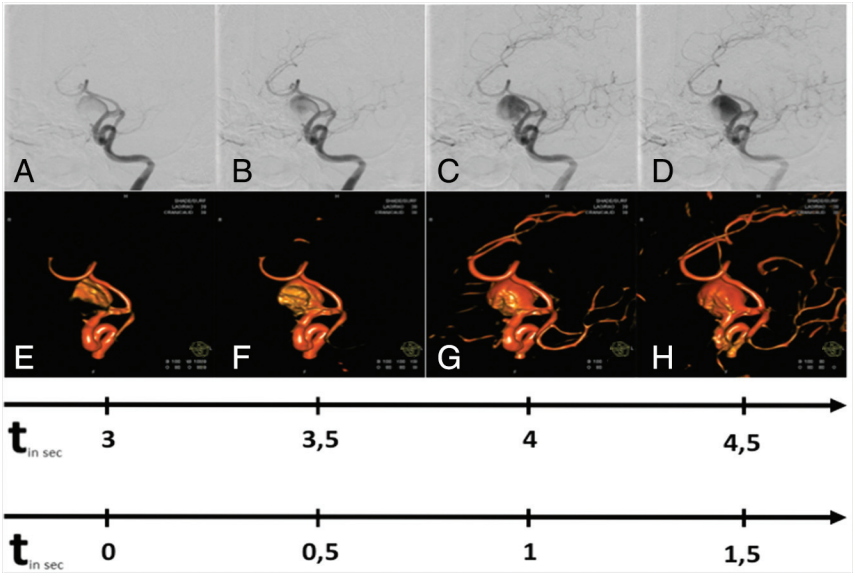

FIG 4. Illustrative case 3. This 73-year-old male patient has visual loss on the left side due to a giant sacciform aneurysm of the left carotid-T. Comparable with 2D DSA (*A–D*, *upper row*), 4D DSA (*E–H*, *lower row*) shows successive intra-aneurysmal filling with contrast medium. The best time for evaluation of the aneurysmal neck was a late arterial volume that shows a fully enhanced aneurysm. Later volumes offer only residual contrast of the aneurysmal sac due to the washout of contrast agent. The upper timeline shows, in real-time, the filling phases; the lower timeline shows the temporal differences between each image.

arteries were not detected in either 2D or 4D DSA datasets due to heavy steal effects caused by high-flow AVMs (MS-S 3; MS-S 4). In 1 dAVF case, lenticulostriate arteries were not clearly identified due to reduced IQ (IQ = 2) caused by movement artifacts during 4D DSA acquisition.

Quantitative Assessment of the Injection Vessel

In all 2D and 4D datasets ($n = 26$), measurement of the diameter of the injection vessel was successfully performed (ICA = 21, VA = 5). Acquired values did not differ significantly ($mean_{2D}$ = 0.45 ± 0.08 cm; $mean_{4D}$ = 0.46 ± 0.09 cm; $P = .039$).

Dose Measurement

The calculated effective dose for the 12s 4D DSA was 1.2 mSv. The rotation angle differed by 60° between 3D and 4D DSA (200° versus 260°) DSA, whereas tube potential and dose per frame were chosen equally.

DISCUSSION

Currently, 2D DSA (in combination with 3D DSA) is regarded as the criterion standard in the diagnostic work-up of cerebrovascular disease.[2,13] However, existing 2D and 3D techniques are limited in different ways. Although 2D DSA offers high spatial and temporal resolution, it is limited by the C-arm system

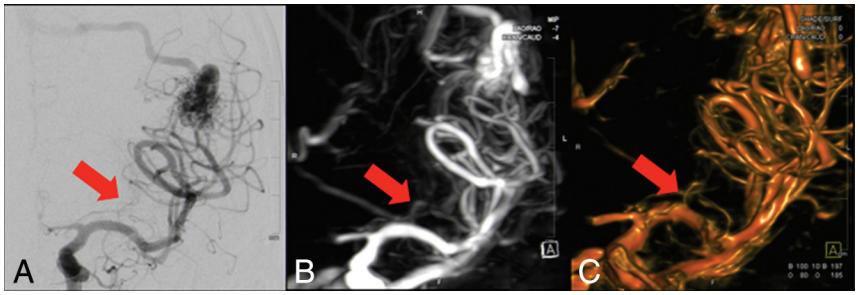

FIG 5. This 52-year-old female patient has an AVM in the left hemisphere with feeders from the MCA territory and superficial drainage. The magnified 2D DSA image (*A*) and the MIP and volume rendered images of 4D DSA (*B* and *C*) of the left-sided anterior circulation demonstrate comparable visualization of lenticulostriate arteries in 2D and 4D DSA (*red arrows*), respectively. Especially, MIP images (*B*) are a helpful tool for identification of perforators.

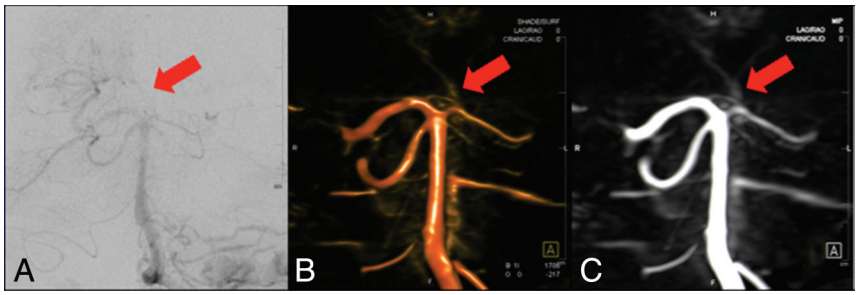

FIG 6. This 59-year-old male patient has pulsatile tinnitus caused by a dAVF (Cognard I) with feeders originating from the posterior meningeal artery and antegrade drainage via the transverse sigmoid sinus. The magnified 2D DSA image (*A*) and the MIP and volume rendered images of 4D DSA (*B* and *C*) of the basilar tip demonstrate comparable visualization of thalamoperforating arteries in both modalities (*red arrows*).

in special projections (eg, with extreme angulation). Despite 3D DSA offering no limitation concerning the choice of projections, this method is limited because of lack of temporal information and consecutive vascular overlap. This limitation is especially true in the case of AVMs and AVFs. Therefore, 4D DSA might be helpful in such tasks as evaluation of the AVM angioarchitecture and details of dAVF filling and drainage because it combines advantages of both techniques.

In our case series, 4D DSA, as a novel imaging technique, was performed successfully in all patients and was suitable for imaging of vascular malformations such as AVMs, cerebral aneurysms, and dAVFs. We describe a possible postprocessing method that offers conventional and time-resolved 3D DSA images with high resolution.

In line with recent literature, qualitative parameters obtained from 4D DSA also demonstrated excellent agreement with 2D DSA in our series regarding image quality and arteriovenous visualization of the angioarchitecture of the pathology. Sandoval-Garcia et al[8] and Lescher et al[9] observed a superior visualization of intranidal structures and the fistulous point of a dAVF, respectively, with 4D DSA because time-resolved 3D imaging enables easy differentiation of arterial and venous structures. We fully agree with the hypothesis of Sandoval-Garcia et al that 4D DSA might simplify the understanding of complex vascular malformations and provides valuable support in risk assessment and therapeutic strategies.[8] Especially after publication of A Randomized Trial of Unruptured Brain Arteriovenous Malformations (ARUBA),[14] an individual assessment of the risk factors regarding hemorrhage has become even more important for generating individual therapeutic strategies.

Previous publications have exclusively analyzed 4D DSA in regard to qualitative parameters.[6-8] To evaluate the accuracy of 4D DSA compared with the current criterion standard (2D DSA), we measured, on the one hand, the maximum diameter of the injection vessel and, on the other hand, specific architectural features of vascular pathologies (eg, nidus size in AVMs, aneurysm size, diameter of the main feeder of a dAVF). Our quantitative evaluation of 4D DSA shows excellent agreement with 2D DSA and demonstrates the reliability of this new technique. However, due to the wide range of possible windowing and missing standardization of the postprocessing, over- and undersizing of vascular structures might be a potential source of error. Moreover, due to the maximum 12-second scan time, 4D DSA could be limited in the visualization of very slow vascular malformations, (eg, low-flow dAVFs, with a bolus passage of >12 seconds). Therefore, 4D DSA might not be considered a substitution for the conventional 2D DSA series, but it has the potential to replace 3D DSA in complex vascular malformations and can help decrease the amount of 2D projections in many cases. Hence, a significant reduction of radiation dose and contrast medium, especially in patients with complex vascular pathologies,[6] is possible. Consequently, this new technique might offer obvious advantages, in particular for young patients or those with renal dysfunction, and might lead to a reduction of the procedural time, which is seen as a protective factor in periprocedural complications.[15]

In contrast to Lescher et al,[9] who observed a limited visualization of small meningeal dAVF feeders, our readers did not feel restricted in identifying even the smallest vessels (eg, lenticulostriate or thalamoperforating arteries). Especially, the use of MIP images can be helpful in differentiating the smallest vessels. Only in cases of heavy steal phenomena ($n = 2$) or movement artifacts ($n = 1$), was visualization of the smallest vessels limited in our series. In our experience, these different findings might refer to different injection protocols (8 seconds in our series versus 7 seconds in the series of Lescher et al) because the duration of arterial contrast could have a significant influence on the IQ and visualization of vessels. Because prolonged injection potentially generates, as also observed by other authors,[8,9] overlapping angiographic phases, further investigation of contrast application to establish optimized injection protocols seems obligatory.

The effective patient dose was measured as 1.2 mSv, which is slightly higher than that of a conventional 3D rotational angiography (0.9 mSv, 5s DSA) and a standard 2D angiographic series

(1 mSv).[11] Similar to 3D rotational angiography, the effective patient dose can be additionally decreased by using collimation, which has not been performed during the dose measurements with the anthropomorphic phantom.[11]

Several noninvasive approaches have tried to generate time-resolved 3D images of the cerebral vasculature. Several authors applied time-resolved MR angiography (4D MRA) with spin-labeling or contrast-enhanced sequences on typical cerebrovascular pathologies and demonstrated high agreement with DSA in hemodynamic information[16] in the assessment of AVMs[17-19] and fistulas.[20-22] 4D MRA seems to be a promising alternative for DSA. In fact, 4D MRA avoids the use of radiation and, in using arterial spin-labeling techniques, contrast agents. However, these techniques are limited in various ways. Compared with DSA, 4D MRA provides reduced spatial resolution[18,22,23] with resulting difficulty in differentiating small arterial vessels[18,21,22] or draining veins.[19,20] Furthermore, ferromagnetic artifacts (eg, retainers, dental implants)[18] and a long acquisition time[20] might contribute to reduced diagnostic quality. Still, recent literature advises performing DSA for definite evaluation of the preferred therapy strategy[17] or the posttherapeutic follow-up of AVMs.[24]

Another encouraging approach is time-resolved CT angiography (4D CTA), which has already found multifunctional applications in cerebrovascular diagnostics (eg, in the evaluation of dAVFs, AVMs, and cerebral collaterals in cases of vessel occlusion).[25] Several publications demonstrated the clinical feasibility[26] and a high agreement between 4D CTA and DSA.[27-29] Although the spatial resolution of 4D CTA is rated higher than that of 4D MRA,[30] both modalities are struggling with the same limitations. Small vessels (eg, tiny feeders of an AVM[27]) and specific angioarchitectural details of dAVFs[29] do not have the same visual quality as in DSA. Willems et al[31] analyzed the value of 4D CTA in the diagnostic work-up of dAVFs in 11 cases. Although both readers fully agreed in 11 cases on an established classification system, there was 1 low-flow fistula that was not detected on 4D CTA at all. Therefore, relying on 4D CTA alone might lead to loss of detailed information (eg, on the exact number of feeders or the exact angioarchitecture of the nidus).

Although data acquisition was successful in all 26 cases, our analysis has several limitations. First, it was limited by the small amount of any pathology. Moreover, any dataset in our series was acquired by selective injections either via the ICA or VA. Therefore, our series does not cover datasets acquired by injection from the subclavian, external, or common carotid artery. Missing standardization for contrast application and postprocessing is the most important limitation of our analysis.

CONCLUSIONS

4D DSA is a promising new method for time-resolved 3D imaging of cerebral vessels that allows visualization of the vascular anatomy comparable with that of 2D DSA with an effective dose within the range of a standard angiographic series. Therefore, 4D DSA might simplify the understanding and improve treatment planning of complex malformations. Furthermore, because the diagnostic information from a 4D DSA was equivalent to that in the 2D acquisitions, we believe that the number of 2D acquisitions required for an examination may be reduced through the use of 4D DSA.

Disclosures: Markus Kowarschik—*UNRELATED: Employment*: Siemens, *Comments*: full-time employee. Charles Strother—*UNRELATED: Grant*: National Institutes of Health.* *Money paid to the institution.

REFERENCES

1. Ogilvy CS, Stieg PE, Awad I, et al; Special Writing Group of the Stroke Council, American Stroke Association. **AHA Scientific Statement: recommendations for the management of intracranial arteriovenous malformations—a statement for healthcare professionals from a special writing group of the Stroke Council, American Stroke Association.** *Stroke* 2001;32:1458–71 CrossRef Medline
2. Oppenheim C, Meder JF, Trystram D, et al. **Radiosurgery of cerebral arteriovenous malformations: is an early angiogram needed?** *AJNR Am J Neuroradiol* 1999;20:475–81 Medline
3. Gandhi D, Chen J, Pearl M, et al. **Intracranial dural arteriovenous fistulas: classification, imaging findings, and treatment.** *AJNR Am J Neuroradiol* 2012;33:1007–13 CrossRef Medline
4. Lauriola W, Nardella M, Strizzi V, et al. **3D angiography in the evaluation of intracranial aneurysms before and after treatment: initial experience** [Article in English, Italian]. *Radiol Med* 2005;109:98–107 Medline
5. Tanoue S, Kiyosue H, Kenai H, et al. **Three-dimensional reconstructed images after rotational angiography in the evaluation of intracranial aneurysms: surgical correlation.** *Neurosurgery* 2000;47:866–71 CrossRef Medline
6. Davis B, Royalty K, Kowarschik M, et al. **4D digital subtraction angiography: implementation and demonstration of feasibility.** *AJNR Am J Neuroradiol* 2013;34:1914–21 CrossRef Medline
7. Sandoval-Garcia C, Royalty K, Aagaard-Kienitz B, et al. **A comparison of 4D DSA with 2D and 3D DSA in the analysis of normal vascular structures in a canine model.** *AJNR Am J Neuroradiol* 2015;36:1959–63 CrossRef Medline
8. Sandoval-Garcia C, Royalty K, Yang P, et al. **4D DSA a new technique for arteriovenous malformation evaluation: a feasibility study.** *J Neurointerv Surg* 2016;8:300–04 CrossRef Medline
9. Lescher S, Gehrisch S, Klein S, et al. **Time-resolved 3D rotational angiography: display of detailed neurovascular anatomy in patients with intracranial vascular malformations.** *J Neurointerv Surg* 2016 Aug 4. [Epub ahead of print] CrossRef Medline
10. Mistretta CA. **Sub-Nyquist acquisition and constrained reconstruction in time resolved angiography.** *Med Phys* 2011;38:2975–85 CrossRef Medline
11. Struffert T, Hauer M, Banckwitz R, et al. **Effective dose to patient measurements in flat-detector and multislice computed tomography: a comparison of applications in neuroradiology.** *Eur Radiol* 2014;24:1257–65 CrossRef Medline
12. **The 2007 Recommendations of the International Commission on Radiological Protection. ICRP publication 103.** *Ann ICRP* 2007;37:1–332 CrossRef Medline
13. Struffert T, Lang S, Scholz R, et al. **Radiation dose in cerebral angiography and flat detector CT applications in neuroradiology** [in German]. *Radiologe* 2015;55:654–62 CrossRef Medline
14. Mohr JP, Parides MK, Stapf C, et al; international ARUBA investigators. **Medical management with or without interventional therapy for unruptured brain arteriovenous malformations (ARUBA): a multicentre, non-blinded, randomised trial.** *Lancet* 2014;383:614–21 CrossRef Medline
15. Bendszus M, Koltzenburg M, Burger R, et al. **Silent embolism in diagnostic cerebral angiography and neurointerventional procedures: a prospective study.** *Lancet* 1999;354:1594–97 CrossRef Medline
16. Robson PM, Dai W, Shankaranarayanan A, et al. **Time-resolved vessel-selective digital subtraction MR angiography of the cerebral vasculature with arterial spin labeling.** *Radiology* 2010;257:507–15 CrossRef Medline
17. Kukuk GM, Hadizadeh DR, Boström A, et al. **Cerebral arteriovenous malformations at 3.0 T: intraindividual comparative study of 4D-MRA in combination with selective arterial spin labeling and digital**

subtraction angiography. *Invest Radiol* 2010;45:126–32 CrossRef Medline
18. Eddleman CS, Jeong HJ, Hurley MC, et al. **4D radial acquisition contrast-enhanced MR angiography and intracranial arteriovenous malformations: quickly approaching digital subtraction angiography.** *Stroke* 2009;40:2749–53 CrossRef Medline
19. Xu J, Shi D, Chen C, et al. **Noncontrast-enhanced four-dimensional MR angiography for the evaluation of cerebral arteriovenous malformation: a preliminary trial.** *J Magn Reson Imaging* 2011;34:1199–205 CrossRef Medline
20. Hori M, Aoki S, Oishi H, et al. **Utility of time-resolved three-dimensional magnetic resonance digital subtraction angiography without contrast material for assessment of intracranial dural arterio-venous fistula.** *Acta Radiol* 2011;52:808–12 CrossRef Medline
21. Iryo Y, Hirai T, Kai Y, et al. **Intracranial dural arteriovenous fistulas: evaluation with 3-T four-dimensional MR angiography using arterial spin labeling.** *Radiology* 2014;271:1939–39 CrossRef Medline
22. Nishimura S, Hirai T, Sasao A, et al. **Evaluation of dural arteriovenous fistulas with 4D contrast-enhanced MR angiography at 3T.** *AJNR Am J Neuroradiol* 2010;31:80–85 CrossRef Medline
23. Raoult H, Bannier E, Robert B, et al. **Time-resolved spin-labeled MR angiography for the depiction of cerebral arteriovenous malformations: a comparison of techniques.** *Radiology* 2014;271:524–33 CrossRef Medline
24. Soize S, Bouquigny F, Kadziolka K, et al. **Value of 4D MR angiography at 3T compared with DSA for the follow-up of treated brain arteriovenous malformation.** *AJNR Am J Neuroradiol* 2014;35:1903–09 CrossRef Medline
25. Frölich AM, Wolff SL, Psychogios MN. **Time-resolved assessment of collateral flow using 4D CT angiography in large-vessel occlusion stroke.** *Eur Radiol* 2014;24:390–96 CrossRef Medline
26. Ono Y, Abe K, Suzuki K, et al. **Usefulness of 4D-CTA in the detection of cerebral dural sinus occlusion or stenosis with collateral pathways.** *Neuroradiol J* 2013;26:428–38 CrossRef Medline
27. Wang H, Ye X, Gao X, et al. **The diagnosis of arteriovenous malformations by 4D-CTA: a clinical study.** *J Neuroradiol* 2014;41:117–23 CrossRef Medline
28. Beijer TR, van Dijk EJ, de Vries J. **4D-CT angiography differentiating arteriovenous fistula subtypes.** *Clin Neurol Neurosurg* 2013;115:1313–16 CrossRef Medline
29. Willems PW, Brouwer PA, Barfett JJ, et al. **Detection and classification of cranial dural arteriovenous fistulas using 4D-CT angiography: initial experience.** *AJNR Am J Neuroradiol* 2011;32:49–53 CrossRef Medline
30. Brouwer PA, Bosman T, van Walderveen MA, et al. **Dynamic 320-section CT angiography in cranial arteriovenous shunting lesions.** *AJNR Am J Neuroradiol* 2010;31:767–70 CrossRef Medline
31. Willems PW, Taeshineetanakul P, Schenk B, et al. **The use of 4D-CTA in the diagnostic work-up of brain arteriovenous malformations.** *Neuroradiology* 2012;54:123–31 CrossRef Medline